The Journal of Experimental Biology 209, 4788-4801
Published by The Company of Biologists 2006
doi:10.1242/jeb.02582

Correlation of C-start behaviors with neural activity recorded from the hindbrain in free-swimming goldfish (*Carassius auratus*)

Shennan A. Weiss[1,*], Steven J. Zottoli[2], Samantha C. Do[1], Donald S. Faber[1] and Thomas Preuss[1]

[1]*Dominick P. Purpura Department of Neuroscience, Albert Einstein College of Medicine, Bronx, NY 10461, USA and*
[2]*Department of Biology, Williams College, Williamstown, MA 01267, USA*

*Author for correspondence (e-mail: sweiss@aecom.yu.edu)

Accepted 4 October 2006

Summary

Startle behaviors in teleost fishes are well suited for investigations of mechanisms of sensorimotor integration because the behavior is quantifiable and much of the underlying circuitry has been identified. The teleost C-start is triggered by an action potential in one of the two Mauthner (M) cells. To correlate C-start behavior with electrophysiology, extracellular recordings were obtained from the surface of the medulla oblongata in the hindbrain, close to the M-axons, in freely swimming goldfish monitored using high-speed video. The recordings included action potentials generated by the two M-axons, as well as neighboring axons in the dorsal medial longitudinal fasciculus. Axonal backfills indicated that the latter originate from identifiable reticulospinal somata in rhombomeres 2–8 and local interneurons. Diverse auditory and visual stimuli evoked behaviors with kinematics characteristic of the C-start, and the amplitude of the first component of the hindbrain field potential correlated with the C-start direction. The onset of the field potential preceded that of the simultaneously recorded trunk EMG and movement initiation by 1.08±0.04 and 8.13±0.17 ms, respectively. A subsequent longer latency field potential was predictive of a counterturn. These results indicate that characteristic features of the C-start can be extracted from the neural activity of the M-cell and a population of other reticulospinal neurons in free-swimming goldfish.

Key words: startle, escape, Mauthner, reticulospinal, medial longitudinal fasciculus.

Introduction

One goal of neuroethology is to account for an innate behavior at the level of single, identified neurons (Bullock, 1990). Fast startle responses have been the subject of a number of studies related to this issue, since in species such as crayfish (Wine and Krasne, 1972; Beall et al., 1990; Edwards et al., 1999), earthworms (Drewes et al., 1978), squid (Otis and Gilly, 1990; Neumeister et al., 2000; Preuss and Gilly, 2000), larval zebrafish (Prugh et al., 1982) and goldfish (Zottoli, 1977; Eaton et al., 1981; Canfield and Rose, 1993), these behaviors seem to be triggered by identifiable cells.

One of the best-characterized startle behaviors in vertebrates is the C-start exhibited by teleosts. There are two sequential stages to the C-start (Domenici and Blake, 1997; Eaton et al., 2001): stage 1, where the head rotates about the center of mass and the fish's body exhibits a curvature that resembles a C, and stage 2, during which the fish propels forward. Sometimes the fish may also rotate in the opposite direction during stage 2, producing a counterturn (Foreman and Eaton, 1993). C-starts in goldfish are initiated by the Mauthner (M) cells (Wilson, 1959; Zottoli, 1977; Eaton et al., 1981), an identifiable pair of large neurons found in the medulla oblongata (Zottoli, 1978). These neurons have been studied extensively and have a number of unique features that make them amenable for the analysis of the neuronal basis of behavior (Faber and Korn, 1978; Zottoli and Faber, 2000; Korn and Faber, 2005). For example, the large extracellular field potential recorded in the vicinity of the axon cap, a structure surrounding the M-cell initial axonal segment, unequivocally allows identification of that cell. Consequently, metal microelectrodes have been implanted near the axon cap, allowing this neuron's activity to be recorded in free-swimming goldfish. It is well established that the M-cell extracellular field potential is correlated with contralateral EMG responses (Zottoli, 1977) and C-starts (Eaton et al., 1981). In translucent larval zebrafish activation of identifiable reticulospinal neurons can be monitored *in vivo* by calcium imaging. These studies demonstrate that stimuli that elicit the C-start activate a distributed population of reticulospinal neurons in parallel with the M-cell (Gahtan et al., 2002). However, because this imaging technique requires that the fish be immobilized it is not yet clear how activation of these neurons correlates with the trajectory and kinematic parameters of the escape behavior. In addition, most of the escapes studied so far have been triggered by abrupt stimuli,

most often mechanosensory. The respective roles of the M-cells and the other reticulospinal neurons in escapes triggered by more gradual and longer lasting stimuli are also not yet established.

One of the earliest attempts to isolate M-cell activity during behavior utilized an electrode implanted into the spinal cord of lungfish (Wilson, 1959). Various stimuli were used to elicit fast tail flexion, which was correlated with a single, all-or-none extracellular spike followed by a graded compound action potential (Wilson, 1959). This technique is attractive since it provides the possibility of recording the collective activity of one or both M-axons and other descending activity in a free-swimming fish. For example, recordings from the surface of the lamprey spinal cord have revealed correlations between descending neuronal population activity and swimming (Deliagina et al., 2000).

The M-axons are visible in the hindbrain on the surface of the medulla oblongata between the vagal lobes in goldfish (Zottoli et al., 1995). At that location the axons are approximately 150 μm below the surface. We have taken advantage of this morphological feature to monitor M-axon activity and that of other descending axons in the medial longitudinal fasciculus (mlf_d) in free-swimming goldfish. The results show that (1) the activity of the two M-axons can be distinguished in field potential recordings from the mlf_d and are correlated with C-start behavior, including its direction; (2) activity of other descending axons, which arise in the rhombencephalic medial reticular zone, is correlated with counterturns following the initial C-bend; and (3) diverse auditory and visual stimuli elicit C-start behaviors triggered by the M-cell. Thus diverse stimuli elicit a stereotypic C-start behavior initiated by the M-cell in concert with a population of other neurons that also may function to mediate counterturns during stage 2 of the escape.

Materials and methods

Adult goldfish *Carassius auratus* L., 5–20 cm in body length, were maintained as previously described (Preuss and Faber, 2003). In general, the larger fish, 15–20 cm, were used for chronic recording experiments.

Elicitation of startle responses and kinematic measurements

The circular experimental aquarium had a diameter of 76 cm and a water depth of 28 cm. Water temperature was maintained at 18°C. C-starts were elicited with sounds generated by software written in Igor Pro. The computer-generated signal was amplified (Servo 120; Samson, Syosset, NY, USA) and produced by an underwater loud speaker (UW-30; University Sound, Buchanan, MI, USA) at the outer circumference of the tank. Sound pulses, i.e. pips, were generated as a single cycle of a 100, 200 or 300 Hz sound wave. Because of reverberation from the walls of the tank and continued vibration of the speaker membrane the sound persisted for multiple cycles with successively longer periods and more distortion. The peak pressure of the pip stimulus occurred at the first or second cycle, depending on the location of the hydrophone, and was 179–185 dB re: 1 μPa in the center of the tank. 200 Hz sound waves 50 or 200 ms in duration that increased in intensity exponentially from zero were also used to evoke escapes. These 'ramped' sound waves were used to elicit escapes because, as opposed to pips, they remain constant in frequency and they proved ideal for studying the auditory processing properties of the M-cell (Szabo et al., 2006). In addition, predatory strikes by other fish that evoke C-starts sometimes do not appear to be sudden strikes but rather consist of progressively more powerful multiple body-bends (Harper and Blake, 1991). The peak of the ramped stimulus occurred at the last cycle and was 179–186 dB re: 1 μPa in intensity in the center of the tank at a distance 44 cm from the speaker membrane. Visual looming stimuli, which also simulate object approach, consisted of a series of computer generated black disks of increasing size projected with a LCD projector (1024×768 pixels, 60 Hz refresh rate) on a white screen ~16 cm above the fish (Fig. 1A). This produces a growing image on the retina, and its size can be quantified as the view angle $\theta=2\times\tan^{-1}(d/2\times s)$, where d is the diameter of the projected disk on the screen and s is the distance from the screen to the eye. Increasing disk size simulates the normally occurring decrease in s, during an approach. Stimuli differed in their projected size, approach velocity and duration (Fig. 1B), as described in detail elsewhere (Preuss et al., 2006). The time intervals between trials varied randomly from 2–20 min. The auditory stimulus was recorded (sampling rate, 30 μs) with a hydrophone (SQ01; Sensor Technology, Collingwood, Ontario, Canada) and the on- and offset of the visual looming stimulus were monitored with a photodiode.

Video recordings were made from the underside of the tank at 1000 frames s^{-1} at a resolution of 512×384 pixels using a

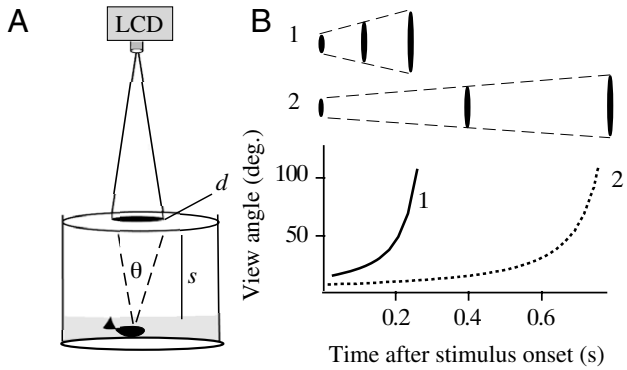

Fig. 1. Illustration of the generation and properties of the visual looming stimulus. (A) An LCD projector projects a black disk that grows in size with time on to a translucent white screen. This produces a growing image on the retina, and its size can be quantified as the view angle $\theta=2\times\tan^{-1}(d/2\times s)$, where d is the diameter of the projected disk on the screen and s is the distance from the screen to the eye. (B) Two looming stimuli 1 and 2, plotted as θ *vs* time. Both have the same final view angle, but stimulus 2 grows more slowly than 1.

high-speed video camera (Kodak Extapro 1000 HRC; Eastman Kodak, San Diego, CA, USA), and were stored digitally. A 1 ms flash from a light-emitting diode outside the tank and not seen by the fish marked the stimulus onset on the video and served as a reference point for latency measurements. For each startle sequence selected, 176 frames (coincident with the onset of the auditory stimulus or 25 frames before the visual response onset) were analyzed. The *x*- and *y*- positions of the head and the center of mass (COM) were measured manually in ImageJ (NIH, Bethesda, MD, USA), or using the automated movement tracking software BIOBSERVE (Bonn, Germany). Visually evoked startles were tracked manually at a lower temporal resolution because the LCD projector produced a flicker effect. When tracked manually, the COM was defined as a point on the midline located between the pectoral fins. Angular and linear displacement plots were calculated from *x*- and *y*-positions of the head using a fixed rectilinear coordinate system. Heading (*H*) is the angle, in degrees, of the midline vector connecting the COM to the tip of the head and was calculated by the equation: $H=\arctan(y_{head}-y_{COM})/(x_{head}-x_{COM})$ at 1 ms intervals for auditory stimuli and 3–5 ms intervals for visual stimuli. Angular velocity (dH/dt) was calculated by fitting the fish's heading as a function of time with a 10th degree polynomial and taking the derivative of this function. Stage 1 was defined as the interval beginning with movement of the head and ending with forward propulsion of the center of mass (COM) by more than 5 mm (Nissanov et al., 1990; Eaton and Emberly, 1991). Other investigators (Domenici and Blake, 1997) classify the end of stage 1 by measuring the latency to the maximal initial rotation.

Statistics and data analysis

All statistical tests were carried out using Statview 5.0 (SAS Institute, Cary, NC, USA) All custom analysis software was written in Labview 7.0. Values are given as the mean ± standard error of the mean (s.e.m.) unless specified otherwise. *N*=number of fish; *n*=number of trials.

Surgery for chronic recordings

Fish were anesthetized during the surgery with continuous perfusion of ice water containing 60 mg l^{-1} MS-222 (3-aminobenzoic acid ethyl ester; Sigma; St Louis, MO, USA). The fish were restrained in a manner similar to that used for acute recording *in vivo* (Preuss and Faber, 2003). When the fish no longer exhibited a motor response to touch of the head and caudal fin, the skin overlying the cranium was removed with a razor blade until the surface of the skull was free of moisture. Two self-threading screws (Stoelting, Wood Dale, IL, USA) were inserted in the skull. A 4 mm×3 mm opening centered at the midline and located just rostral to the suture between the occipital and parietal bones was drilled and lipid droplets overlying the brain were removed by aspiration. Electrode penetration was in the rostral–caudal direction at an angle of approximately 60–70° from the horizontal. The electrode tip was positioned 100–300 μm lateral to the midline and just caudal to the facial lobe, at the brain surface and lowered to a depth <300 μm. The M-axons are visible in this region with the aid of a dissecting microscope. Microelectrodes were prepared from Teflon coated 316 stainless steel wire 100 μm in diameter (California Fine Wire Company, Grover Beach, CA, USA) with 0.5–1.0 mm of the tip stripped of insulation or the tip cut with a pair of fine scissors. Both techniques yielded comparable results. Impedance measurements ranged from 30–40 KΩ at 1 kHz. A stainless steel wire stripped of insulation at its tip and wrapped around the metal skull screws served as a reference. After positioning the recording electrode, the cranium was filled with mineral oil. The electrode was fixed in position with a combination of cyanoacrylate and dental cement. EMG electrodes were prepared from 40 μm steel alloy (Stablohm 800A, California Fine Wire Company, Grover Beach, CA, USA) with 2–5 mm of insulation removed using a razor blade. The deinsulated tips were bent at the ends and fed into a syringe needle. The needle, with the electrodes inside, was inserted in dorsal white musculature two scale widths dorsal to the visible band of the posterior lateral line and near the midpoint of the rostral–caudal axis. The electrodes were held in place by a drop a cyanoacrylate adhesive on the epidermis with the overlying scales removed.

Activity from the hindbrain of ten free-swimming goldfish was successfully recorded; other fish were unable to maintain equilibrium following the surgery, presumably due to inadvertent damage to the semicircular canals. Experiments were initiated 2–5 h post operatively. The leads connecting the brain and EMG electrodes were several feet in length. During the experiment wires were occasionally manually detangled. Evoked startle responses in which tangled leads restricted the fish's movement or resulted in cross-talk were excluded from analysis. Following chronic recordings, in some experiments, the fish was re-anesthetized with MS-222 and immobilized with curare. The spinal cord was exposed and extracellular responses to antidromic stimulation were recorded from the implanted electrode.

Electrophysiology

Extracellular responses were amplified 1000× with a 4-channel differential AC amplifier (Model 1700, A-M Systems, Carlsborg, WA, USA) and bandpass filtered from 100 Hz–20 kHz. EMG responses were amplified 100× and bandpass filtered from 300–10 kHz. In a subset of experiments, in curarized fish, simultaneous recordings were obtained intracellularly from the M-cell soma and extracellularly from the hindbrain. For this purpose we used previously described methods for the intracellular recording (Preuss and Faber, 2003). Briefly, an antidromic stimulus was generated by a bipolar stimulating electrode placed on the spinal cord and M-cell responses were recorded with a 2–7 MΩ glass micropipette containing 5 mol l^{-1} potassium acetate or 3 mol l^{-1} KCl. Data were recorded online with a Macintosh G4, using acquisition software developed in the laboratory for Igor Pro (Wavemetrics, Lake Oswego, OR, USA) at a sampling interval of 10–50 μs, and analyzed with the same software and Labview 7 (National Instruments, Austin, TX, USA).

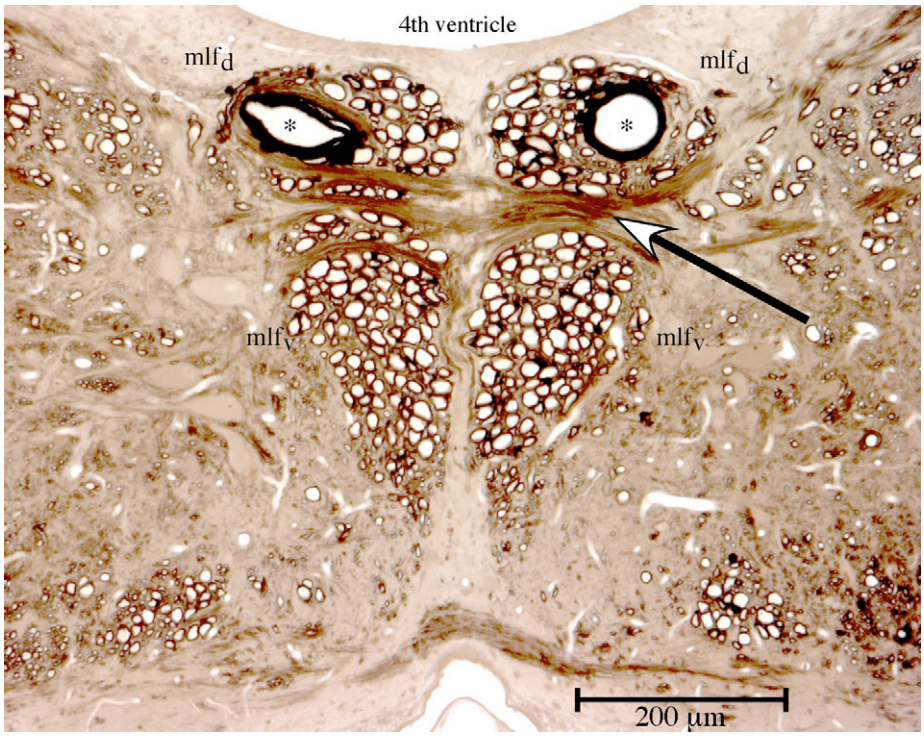

Fig. 2. Myelinated axons at the level of the recording site, 5 μm transverse section 500 μm posterior to the caudal edge of the facial lobe. The mlf is on either side of the midline. The dorsal portion, mlf$_d$, contains the large M-axon (asterisk) and is separated from the ventral portion, mlf$_v$, by a commissure (arrow). The surface of the hindbrain and the 4th ventricle are dorsal to the M-axons.

Morphology of the axons in the mlf$_d$

One goldfish (5 cm body length) was anesthetized in 0.03% MS-222 and perfused intracardially with fixative (2.5% glutaraldehyde, 1% paraformaldehyde in 0.1 mol l^{-1} sodium cacodylate buffer, pH 7.4). The brain was removed, dissected and post-fixed for 1 h, washed in 0.1 mol l^{-1} cacodylate buffer, post-fixed in 2% OsO_4 in 0.1 cacodylate buffer for 4 h, washed, dehydrated in a graded ethanol series, cleared in propylene oxide and embedded in Epon. The brain was serially sectioned (5 μm) in the transverse plane. Unstained sections were mounted on glass slides for analysis and photographed (Zeiss Axiocam digital camera).

Axons of the right and left dorsal portion of the mlf$_d$ were drawn from six consecutive sections with the aid of a camera lucida, starting 500 μm caudal to the posterior edge of the facial lobe (close to the site of chronic recordings). The drawings were used to determine the number of axons 10 μm and larger in diameter not including sheath thickness. Only axons present in all six sections were counted. Since smaller axons could not be easily traced from section to section, their number was based on measurements of the sixth section only.

The boundaries of the mlf$_d$ extended laterally from the midline to the far edge of the M-axon and ventrally from the ventricle to the commissure that separates the dorsal from the ventral portions of the mlf, i.e. the mlf$_v$ (Fig. 2).

Cells of origin of the mlf$_d$

To identify the somata of origin that give rise to axons in the mlf$_d$, Lucifer Yellow (Sigma) was injected into axons adjacent to the M-axon in 16 fish. In order to obtain a more general view of the cells of origin, in three experiments a population of damaged axons was filled using dextran biotin (10 k, Invitrogen, Carlsbad, CA, USA).

In the Lucifer Yellow experiment, the M-axon was filled first, followed by injection into one or more adjacent axons. For this purpose a glass microelectrode (~30 MΩ) was filled with 5% Lucifer Yellow in distilled water. In addition to visually positioning the electrode in the M-axon, identification of the M-axon required the electrode could be raised and lowered approximately 50 μm without change in resting potential Lucifer Yellow was then injected (25–50 nA for 200 ms three times per second for a minimum of 30 min). Fish were perfused with 100 ml of freshwater teleost saline (pH 7.4), followed with 100 ml of 10% formalin in 0.1 mol l^{-1} phosphate buffer (Fisher, Fairlawn, NJ, USA). The brains were removed and placed in fresh fixative overnight, dehydrated and cleared in methyl salicylate before observation under the fluorescence microscope. The distance between the M-cell initial segment and the soma of the non-M-cell was measured in 16 brain whole mounts. These measurements were used to determine the location of the other neuron relative to a particular hindbrain segment. The neurons were identified using previously defined descriptions (Lee et al., 1993). After the brains were viewed in wholemount, they were embedded in paraffin, sectioned transversely at 15 μm, soaked in xylene and coverslips placed on top using a nonfluorescent mounting medium (Eukitt; O. Kindler; distributed by Calibrated Instruments).

To label multiple axons in the mlf$_d$, including the M-axon, a blunt glass microelectrode placed over the right M-axon, was lowered 200–300 μm below the surface and withdrawn, and this protocol was repeated as the electrode was moved medially

in 20 μm steps to the midline. Dextran biotin crystals on the tip of an insect pin were then applied to the lesioned region.

One day post-operatively the goldfish was anesthetized and perfused intracardially with fixative (4% paraformaldehyde, 0.1% glutataldehyde in 0.1 mol l^{-1} phosphate buffer, pH 7.4). The brains were removed, post-fixed for 1 h in the fixative, washed in 0.1 mol l^{-1} phosphate buffer and placed 30% sucrose in 0.1 mol l^{-1} phosphate buffer. The brains were frozen and cryosectioned (60 μm) in the transverse plane and exposed to ABC (Vectastain, Vector Labs, Burlingame, CA, USA) and reacted with diaminobenzidine with nickel ammonium sulfate (Bass et al., 1994). The sections were mounted on gelatin-coated slides and once dry were counterstained with Cresyl Violet Acetate.

Results

Description of the recording site and identification of axons adjacent to the M-axon

We chose to implant the recording electrode in the hindbrain because the M-axon courses close to the surface there and the adjacent axons might participate in the C-start. Therefore, we first asked what neurons might be involved, based on their presence in the mlf_d. The mlf_d on each side of the midline contains about ~80 axons on either side of the midline. There are a number of relatively large myelinated axons medial and ventral to the M-axon (Fig. 2). In the one fish studied quantitatively this tract contained 32 axons with diameters ≥10 μm on the left and 35 on the right.

The dextran biotin backfilling experiments revealed the segmental distribution of cells with axons in the mlf_d (Fig. 3A). In order to determine the distribution of the somata of origin of these mlf_d fibers, we analyzed one of the three brains that had the most intense label and in which inspection of the lesioned region confirmed it was restricted to the mlf_d.

In this case, 72 somata were backfilled. They were localized to the midbrain nucleus of the mlf and throughout the rhombencephalic medial reticular zone (Table 1). Twenty neurons were located in the nucleus of the mlf, two were vestibulospinal neurons, and 50 were reticulospinal cells. Of the latter, 29 were ipsilateral to the injection site while the other 21 were located contralaterally. Some of the neurons could be identified using published descriptions (Lee et al., 1993). Examples of reticulospinal neurons in different rhombomeres are shown in the transverse section in Fig. 3Bi–iv.

Injection of Lucifer Yellow into the axons adjacent to the M-axon often filled both reticulospinal neurons (Fig. 4Ai) and T-reticular interneuron axons (Kimmel et al., 1985), also known as cranial relay neurons (Hackett and Faber, 1983). One vestibulospinal neuron was labeled in this limited sample. Based on the distance between the M-cell initial segment and the soma of the non-M-cell, the 16 cells were assigned to a rhombomere (Table 1). For example, the reticulospinal neuron in Fig. 4Ai–iii was 794 μm caudal to the M-cell's initial segment, placing it in r6. Two other examples of reticulospinal neurons that have crossed axons and are located in r6 are given in Fig. 4Bi,ii. These two, as well as the neuron in Fig. 4Aii,iii, might be MiD3cm the M-cell homologue located in r6 (Lee et al., 1993).

Identification of the M-spike in field potentials evoked by antidromic and orthodromic stimulation of the M-cell

Before attempting the chronic recordings we first asked whether the action potentials generated by either one or both M-axons could be discriminated from recordings obtained with the extracellular electrode placed on the surface of the hindbrain. For this purpose, a second intracellular electrode was located in the M-cell soma and it was stimulated both orthodromically and antidromically in a curarized fish (Fig. 5A). The simultaneous paired recordings allowed a direct

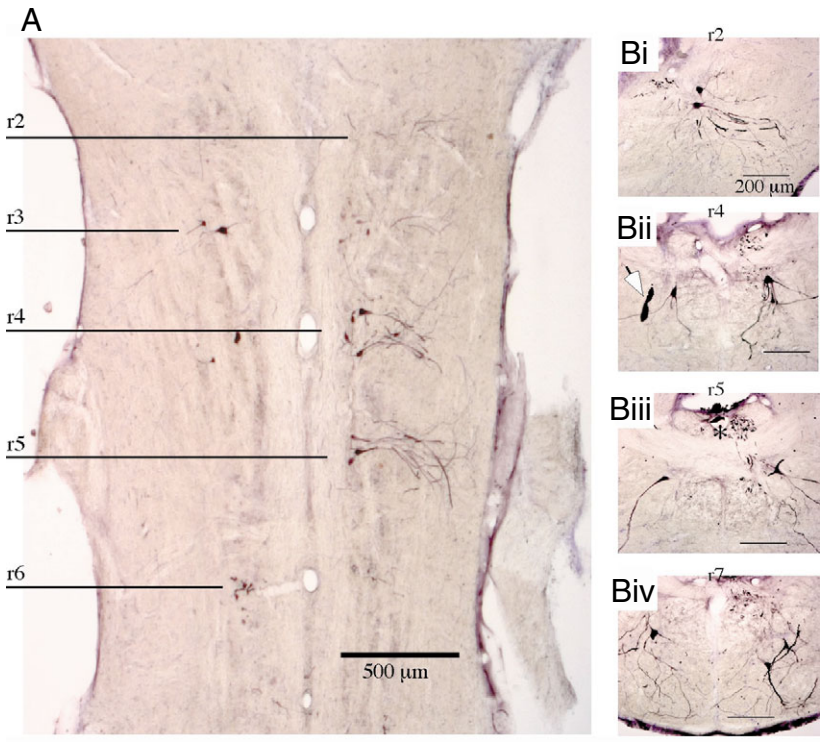

Fig. 3. Reticulospinal somata backfilled with dextran biotin from near the chronic recording site. (A) Horizontal section highlighting hindbrain segmentation. Reticulospinal neurons ipsilateral to the injection site are seen in rhombomeres (r-) 4 and 5 and contralateral in r3, r4 and r6 (Bi–Biv). Transverse sections of representative reticulospinal neurons in r2, r4, r5 and r7, respectively. (Bi) Two ipsilateral reticulospinal neurons in r2. (Bii) Bilateral reticulospinal neurons labeled in r4. Note the Mauthner cell ventral dendrite on the left (arrow). (Biii) Bilateral reticulospinal neurons in r5 at the level of the decussation of the M-axons (asterisk). (Biv) Bilateral reticulospinal neurons located in r7. Midline is to the left in Bi and is centered in Bii–Biv.

Table 1. *Location and identity of Dextran (D-) and Lucifer Yellow (L-) filled somata*

Brain stem location of somata	Number of D-filled somata		Identity of D-filled somata	Number of L-filled somata		Identity of L-filled somata
	Ipsi	Contra		Ipsi	Contra	
Hindbrain						
r2	3	0	RoM2		1	
r3	3	2	RoM3		1	
r4	8	2	M-cell, MiM1D, MiV1	1	1	
r5	5	3	MiD2im, MiD2cm, MiV2	1	3	MiD2cm and/or MiD2cl
r6	3	1	MiV3		6	MiD3cm and/or MiD3ci
r7	5	4	CaD, CaV		1	
r8	2	9	Ca2D, Ca2V			
Vestibulo-spinal nuclei	1	1		1		
Midbrain (nucleus mlf)	20		MeM, MeL			

The neurons are named according to a previously established nomenclature (Kimmel et al., 1982; Metcalfe et al., 1986). The first two letters code the position in the hindbrain: Ro, rostral; Mi, middle; Ca, caudal. The third letter the position of the cell within its segment: D, dorsal; V, ventral; L, lateral; M, medial; I, intermediate. The number following the first three letters codes the segment level in the region. An uppercase letter following the number indicates the position of the neuron relative to another on the same axial level. Lowercase letters at the end denote if the axonal projection are contralateral (Contra; c) or ipsilateral (Ipsi; i) and if the fibers course through the mlf (m) or llf (l).

temporal correlation of M-cell spikes with the recorded extracellular field potential.

The antidromic response in the extracellular recordings consisted of a composite field potential with at least two components, an all or none short latency spike-like component (662±40 μs, *N*=4 fish), followed ≈1 ms later by a complex series of waves (Fig. 5B). When the intensity of stimulation was increased a second all or none component was added to the short latency response and there was a graded increase (not shown) in the amplitude of the longer latency component. A field potential with these characteristics could be measured across a 800 μm width of the hindbrain (Fig. 5Ci) and at various depths (Fig. 5Cii), although it is not clear whether the blunt tipped electrode penetrated into the tissue. The initial component had the same threshold intensity (in V) and latency as the intracellularly recorded antidromic M-spike. The longer latency components of the population response are most likely generated by the activation of nearby fibers in the mlf_d such as the axons of other descending reticulospinal neurons as well as neurons postsynaptic to the M-axon, such as the T-reticular interneuron axons.

To confirm the identification of the short latency component, the M-cells were also stimulated orthodromically using two independent techniques. First, the cell was depolarized past

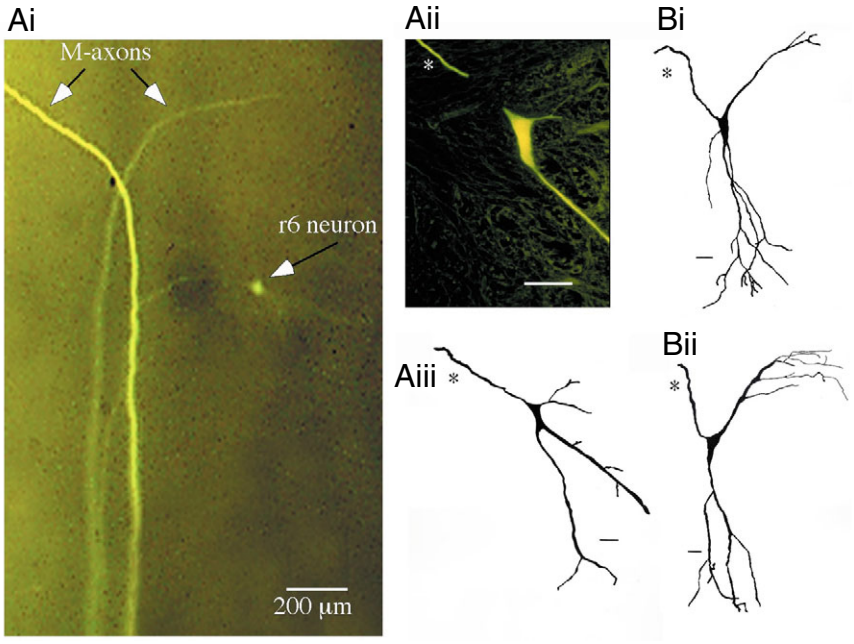

Fig. 4. Segmental localization and reconstruction of reticulospinal neurons with contralateral axons adjacent to the M-axon in the mlf_d. (Ai) Whole mount of the hindbrain, with Lucifer Yellow filled M-axons (upper arrows) and one reticulospinal neuron located in r6 (lower arrow). The M-cell somata are not filled. Higher magnification of the same r6 reticulospinal neuron obtained after sectioning the hindbrain (Aii) and a camera lucida reconstruction of this neuron (Aiii). (Bi,Bii) reconstruction of two other r6 neurons from separate fish. In Aii-Aiii and Bi-Bii, the crossing axons of the reticulospinal neurons are labeled with asterisks, the midline is to the right and scale bars are 50 μm.

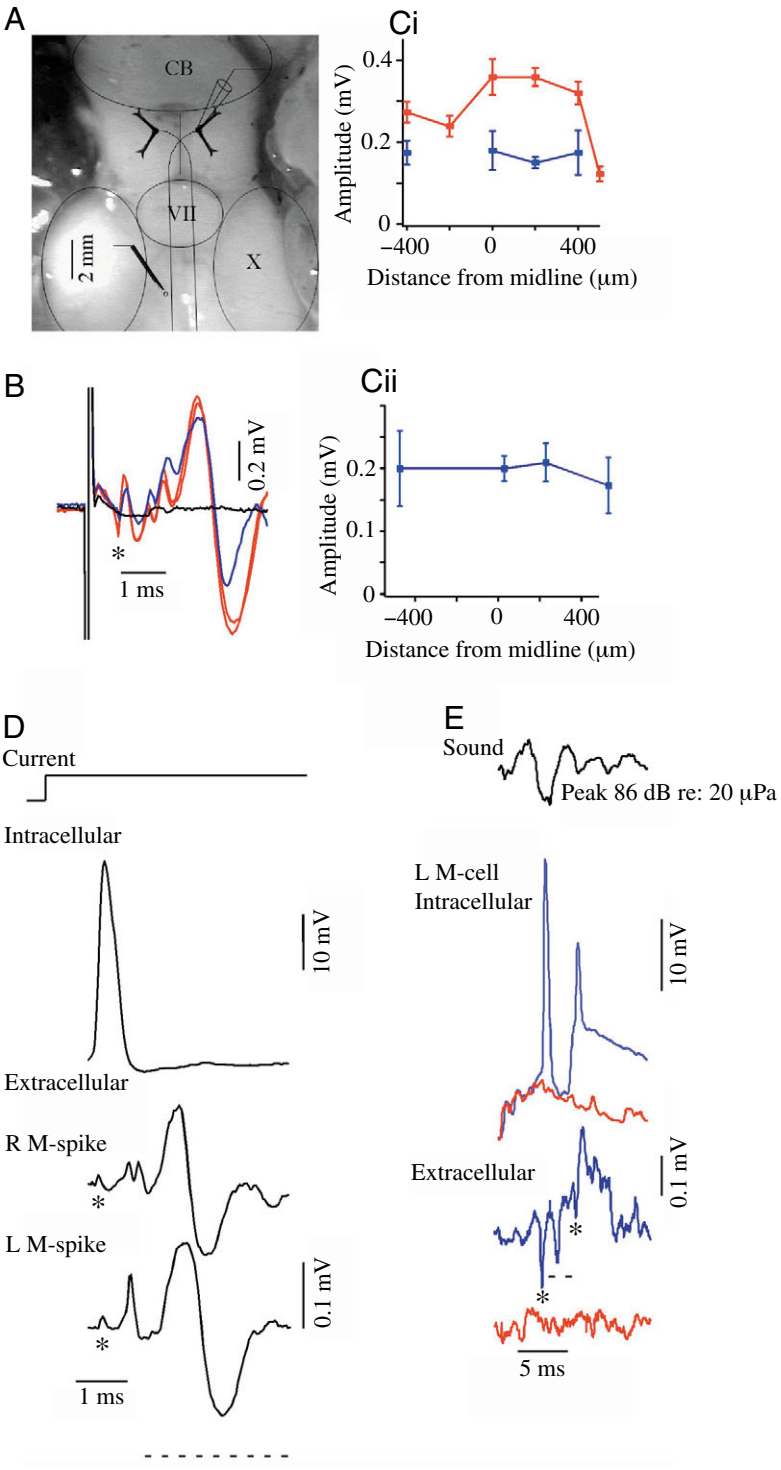

Fig. 5. Discrimination of the M-spike with extracellular recordings in caudal hindbrain. (A) Schematic representation of the experimental arrangement, superimposed drawings of the M-cells onto the medulla oblongata with simultaneous paired intra- and extracellular recording were used for B–E. CB, cerebellum; VII, facial lobe; X, vagal lobes (B,Ci,Cii) Extracellular responses recorded close to the left M-axon. Stimulus intensity was gradually increased from subthreshold for both M-axons (black), to above threshold for one (blue) or both (red). Asterisk indicates M-spike(s). (Ci,Cii) Amplitudes of the surface M-spike fields in B as functions or recording distance from the midline of the caudal hindbrain (Ci) and the amplitude of the single spike at the midline as a function of depth from the surface (Cii). Negative depths are in the saline superfusate. (D) Hindbrain field potentials evoked by orthodromic M-cell activation. Suprathreshold current injection in the left M-cell soma (top), and the corresponding M-axon spike and compound action potentials in the hindbrain (middle). After moving the intracellular electrode to the left M-soma (not shown), the directly activated left M-axon spike and compound field potentials was recorded instead (asterisk) (bottom). Asterisk and horizontal broken line indicate M-axon spike and M-triggered activity, respectively. (E) Compound fields correlated with sound evoked M-cell spike activity. The sound stimulus (top) evoked an EPSP recorded from the M-soma before (red) and after (blue) Cl^- injection; (bottom) corresponding fields recorded in the hindbrain. Note the two M-spikes (asterisks) are separated temporally by M-triggered activity (broken line).

threshold using intrasomatic current injection (Fig. 5D). The somatic M-spike, generated in the initial segment of the axon (Funch and Faber, 1982) and the hindbrain field potential occurred simultaneously. Following orthodromic stimulation of the right M-cell the micropipette was repositioned in the left M-cell soma and when the same procedure was repeated, the orthodromic M-spike was again associated with a hindbrain field potential. Note that in both examples (Fig. 5D), the evoked field potential consisted of the initial M-spike followed by a larger response with a delay of ~1.5 ms, which is likely generated by a population of reticulospinal, motoneurons and local interneurons triggered by the M-spike. Antidromic and orthodromic evoked extracellular M-spikes differed in amplitude and waveform.

Second, the M-cell could also be excited orthodromically with sound stimuli in air (Fig. 5E). Loud abrupt sounds in air (peak 84 dB re: 20 μPa) resulted in 5–10 mV depolarizations in the M-cell soma but did not excite the cell to threshold. In that case, no obvious field potential was generated in the hindbrain. Chloride ions were then injected iontophoretically into the M-cell to shift this ion's equilibrium potential in the depolarizing direction. Consequently, sound evoked inhibition converted to excitation and summed with the afferent excitatory input, such that a loud sound could then excite the M-cell past threshold. The resulting M-spike and M-spike triggered activity could be detected with the hindbrain surface electrodes as distinct field potentials (Fig. 5E). The mean delay from the M-spike to the M-triggered activity was 1.58±0.11 ms (N=7).

In one experiment, the orthodromic and antidromic M-spikes were too small in amplitude to discriminate from background noise. However, the M-spike triggered activity was still present suggesting that even when the electrode was poorly positioned

Table 2. *Comparison of C-start kinematics evoked by different stimuli*

	n	Turn angle (deg.)	Angular velocity (deg. ms^{-1})	Stage 1 duration (ms)	Distance moved (mm) [70 ms]	Distance moved (mm) [100 ms]
Sound pip	28	114.7±8.82	4.3±0.32	11.3±0.80	61.9±3.24	82.3±4.17
200 Hz sinusoid	20	114.8±10.21	4.2±0.32	12.1±0.86	72.4±8.09	91.6±7.41
Visual looming	27	103.4±7.34	3.0±0.10	11.9±0.86	57.0±2.92	83.6±5.0
Implanted fish, pooled	15	70.8±7.53	3.5±0.34	17.8±1.59	47.7±4.35	–

Kinematic parameters were measured from freely swimming goldfish and fish implanted with an electrode in the hindbrain. Data from implanted fish are pooled, independent of the type of stimulus used.

Values are means ± s.e.m.; – not calculated.

M-spike triggered activity could still be detected. Overall, the experiments indicate that the short latency response in the hindbrain field potential is consistently correlated with the M-cell action potential, and that the amplitude of the response allows for the discrimination of the spikes generated by the two M-axons in these acute preparations.

Field potentials associated with evoked C-starts

We analyzed a total of 185 startles in 10 fish implanted with an electrode on the surface of the hindbrain. Startles were evoked by abrupt single cycle sound pips, ramped sound waves, or visual looming stimuli. As described in detail in a subsequent section, kinematic parameters calculated from a random cross section of these startles (n=15), evoked by all three types of stimuli, indicate that they were typical C-starts (Table 2) (Nissanov et al., 1990; Eaton and Emberley, 1991; Zottoli et al., 1999; Preuss and Faber, 2003). Every C-start was associated with an evoked field potential and when the stimulus failed to evoke a startle there was also no evoked field. The amplitude and waveform of the evoked field potential varied across fish because of differences in electrode placement.

The results of Fig. 5 suggest it might be possible to distinguish spikes generated by the left and right M-cells on the basis of their different amplitudes, especially if the recording electrode is not on the midline. In confirmation, the amplitude of the first component of the evoked field potential was correlated with the direction of the C-start in successive trials, in three fish (two tailed student's t-tests; P<0.0001, n=17,19,51, respectively). In two of these experiments the initial 2 and 5 trials, respectively, did not exhibit the observed relationship. This discrepancy likely resulted from changes in the position of the electrode tip. Specifically, in fish in which the electrode was implanted to the left of the midline, the first component was larger in amplitude when the fish made a C-start to the left (Fig. 6Ai,ii). The opposite was the case when the electrode was implanted to the right of the midline (Fig. 6Bi,ii). The amplitude and waveform of the first component of the field potential were independent of the type of stimulus used to evoke the C-start, e.g. pip *vs* ramped sound waves (Fig. 6Aiii,iv) or visual looming stimuli (Fig. 6Biii,iv). Note that the ramped stimulus is constant in frequency throughout its duration, as opposed to the pip, which is distorted (Fig. 6Aiii,iv and Fig. 7A,B). These results strongly suggest that the first component of the evoked field potential is the M-spike.

However, the recorded M-spike could not be stereotyped between fish. It could be either biphasic as in Fig. 6Ai,Bi (peak-to-peak amplitude 135.51±14.02 μV; N=3, n=76), or monophasic as in Fig. 7A,B (peak amplitude of 28.0±0.96 μV; N=7, n=114). In experiments with simultaneous EMG recordings, the M-spike preceded the onset of a large synchronous EMG in the mid trunk musculature by 1.08±0.04 ms (N=3, n=30), consistent with previous reports (Zottoli, 1977). Furthermore, when the different stimuli were used in the same experiment, the evoked M-spikes were comparable, as shown in Fig. 7A,B for C-starts evoked by auditory pips and ramped sound waves, respectively. A similar result was obtained when comparing auditory and visually evoked C-starts. In addition, there was no stimulus-dependent difference in the time interval from the M-spike to EMG onset for the different stimuli (Kruskall–Wallis test, P>0.5, ANOVA F=0.8328, d.f.=2, P=0.47; pip n=14; ramped n=10; visual looming n=5). It remains possible that later components of the evoked field potentials may not be entirely generated by neural activity and may in part be generated by volume conducted muscle activity (Fig. 7A,B). Volume conduction of muscle activity was observed by others using comparatively higher impedance electrodes to chronically recording from the M-cell axon cap (Zottoli, 1977; Eaton et al., 1981).

The delay from the M-spike to the first detectible movement averaged 8.13±0.17 ms for 185 C-starts. This value is consistent with reported delays between the M-spike recorded from the axon cap and movement onset (Zottoli, 1977; Eaton et al., 1982) and thus further supports the notion that the first component of the field potential is the M-spike. In addition, the time interval was stimulus-independent (ANOVA; F=2.091, d.f.=4, P=0.08; Table 3).

Stimulus-dependent differences in the latency of the M-spike reflect differences in how the M-cell processes these stimuli (Preuss and Faber, 2003; Preuss et al., 2006). In implanted fish the latency from stimulus onset to the M-spike was 8.61±0.2 ms (n=160) in C-starts evoked by pips. To determine whether the frequency of a pip stimulus influences the timing of the M-spike C-starts were evoked with three different pip frequencies. While the mean M-spike latency did decrease for pips of increasing frequency (Table 3) the differences were

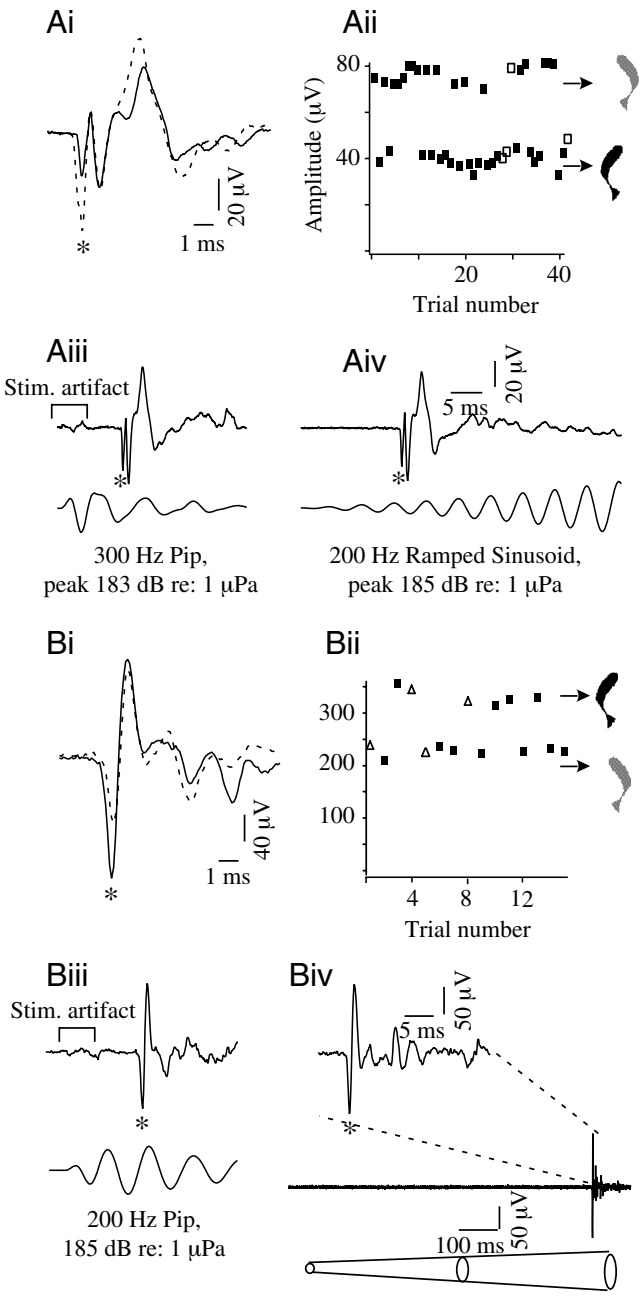

Fig. 6. Discrimination between left and right M-axon activity. Ai–Aiv and Bi–Biv are from two separate experiments, with the implanted electrode closer to the left or right M-axon, respectively. (Ai,Bi) Superimposed fields obtained when the fish turned to the right (solid trace) or to the left (broken trace). Note that in each case the larger M-spike corresponds to activation of the closer M-axon. (Aii,Bii) Plots of M-spike amplitudes *versus* trial number. Silhouettes demonstrate corresponding C-start direction. Closed square, open square, and open triangle indicate pip, ramped sound wave or visual looming stimuli, respectively. (Aiii,Aiv,Biii,Biv) Examples of responses associated with C-starts away from the side of the implanted electrode, i.e. to the right and left, respectively. Stimuli were sound pips in Aiii,Biii, a ramped sound wave in Aiv, and a visual looming stimulus in Biv; asterisk indicates M-spike.

Table 3. *M-initiated complex and movement latency associated with different stimuli*

Stimulus	*n*	Field potential onset latency (ms)	Field potential to movement onset (ms)
100 Hz pip	10	9.9±0.94	8.6±0.924
200 Hz pip	99	8.9±0.26	7.9±0.24
300 Hz pip	51	7.7±0.29	8.0±0.34
Ramped stimuli	15	13.7±1.70	9.7±0.38
Visual looming	10	32–743	8.2±0.74

Summary of all chronic recording experiments (N=10). Data on C-starts evoked by different stimulus parameters were pooled in the cases of ramped and visual looming stimuli. Values are means ± s.e.m., except for field potential onset latency for C-starts following visual looming stimuli, which is expressed as a range.

insignificant (ANOVA F=0.412, d.f.=2, P=0.66). On the other hand the latency from the onset of the computer-triggered 200 Hz ramped sound signal to the M-spike was 13.71±1.7 ms (n=15), which was significantly longer than the latency of startles evoked by sound pips (n=160, Student's t-test; P<0.0001; Table 3). This difference was expected, since for at least its first few cycles the ramped stimulus is much weaker than the pip. The onset latency for the M-spike evoked by a heterogeneous group of visual looming stimuli ranged from 32–743 ms (n=10; Table 3), reflecting processing time in the retina and optic tectum. In trials with a fixed set of visual stimulus parameters (800 ms duration; angular retinal size of the falling disk, i.e. view angle 4–90° with respect to the fish eye), the latency was less variable, namely 731.04±12.06 ms (n=4). The latency of the startle evoked by visual looming stimuli is optimized for collision avoidance and depends on a dynamic scaled function of the view angle (Preuss et al., 2006).

Kinematics of C-starts in non-implanted fish

This study used three types of stimuli, and the chronic recordings indicate that all evoke an M-initiated C-start. If this is the case, these behaviors should have the same kinematic properties. Therefore, 75 startle responses evoked by diverse stimuli were analyzed in 11 non-implanted fish. Each startle was evoked when the fish was near the middle of the tank and was filmed at high magnification. Multiple kinematic parameters from each startle were calculated and compared across stimulus conditions. We also examined the distribution of individual kinematic parameters for evidence of multiple distinct behaviors. For this purpose, a randomly selected subset of previously analyzed visually evoked responses (Preuss et al., 2006) were selected and reanalyzed with the new algorithm, used to generate additional kinematic parameters.

In addition to stage 1 duration and peak angular velocity, which have been used previously to distinguish C-starts from other startle behaviors (Domenici and Batty, 1997; Hale, 2002), three other parameters were used: distance traveled by the center of mass (COM) at 70 and 100 ms, and total turn angle. The dependency of each on stimulus type examined by MANOVA revealed a significant effect of the stimulus (Wilks'

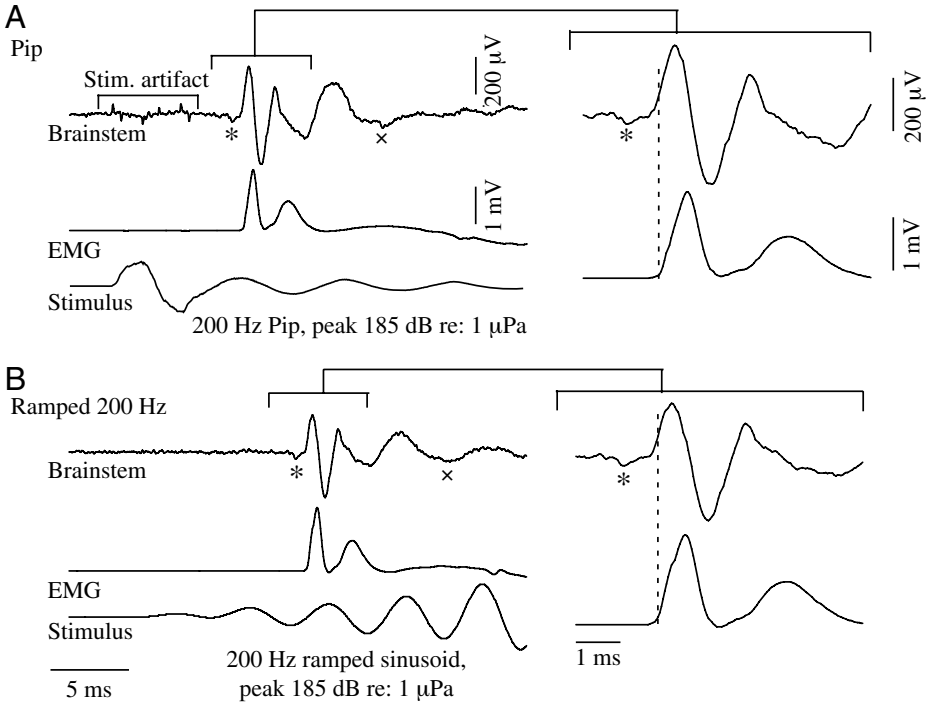

Fig. 7. Simultaneous recordings of the hindbrain field potential and the trunk EMG during C-start escape evoked by a pip (A) or a ramped 200 Hz sound wave (B). Asterisks and crosses indicate M-spike and movement onset, respectively. Right panels show evoked fields at an expanded time scale, vertical dotted line indicates estimated time of EMG onset.

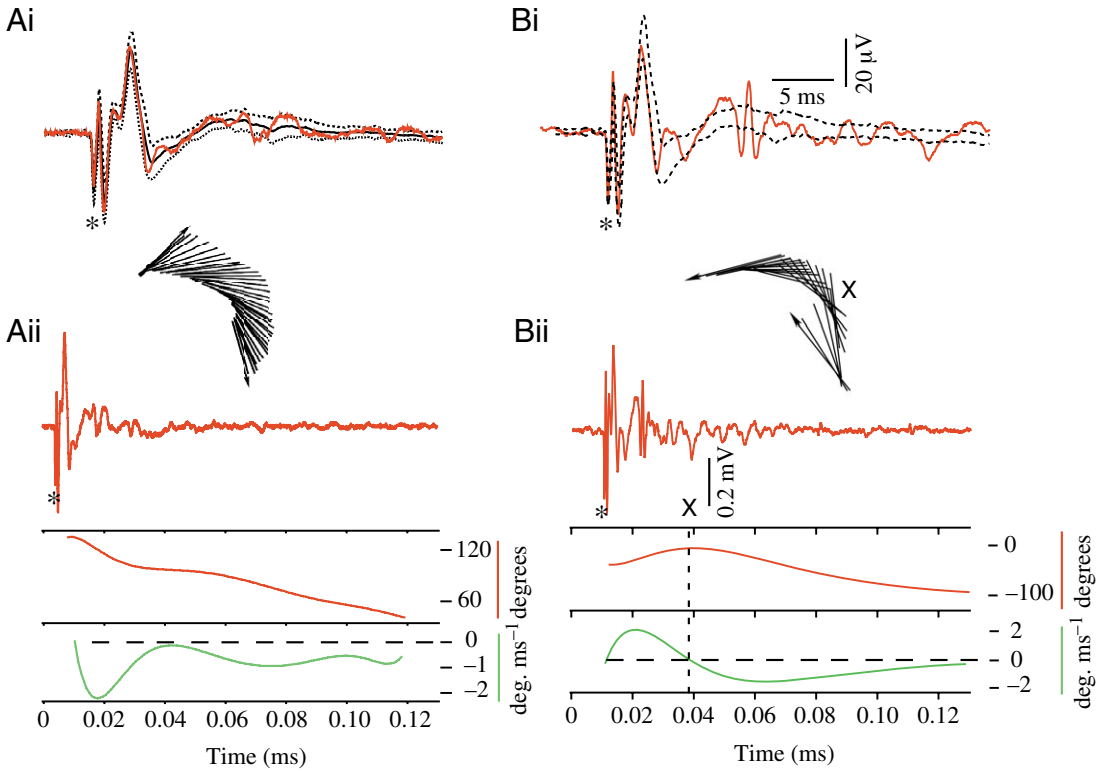

Fig. 8. Correlation between longer latency hindbrain field potentials and C-start trajectories with counterturns. (Ai) Representative field potential (red) associated with a C-start to the right superimposed on the mean for all right responses (n=30) ± 1 s.d. waveform. Asterisk indicates M-spike. (Aii) Top: same field potential as in Ai but at a compressed time scale. Insert above: composite plot of the fish's heading at 5 ms intervals. Middle and bottom: fish heading (red) and angular velocity (green) during the corresponding C-start. (Bi,Bii) Same format as for Ai,Aii but in this case, the selected response (red) deviated from the population mean by more than 1 s.d. ~12 ms after the M-spike (Bi) and was associated with a counterturn (Bii).

Lambda test, F=3.404, P=0.006). However, of these five kinematic parameters, all but the angular velocity (P<0.01) were independent of the stimulus type. In the case of angular velocity, the mean value for startles evoked by visual stimulation (3.03±0.10 deg. ms^{-1}, n=28) was significantly smaller than those of startles evoked by pips (4.33±0.33 deg. ms^{-1}, n=27) or by ramped 200 Hz sound waves (4.158±0.32 deg. ms^{-1}, n=20). This difference was not apparent in the previous analysis of a larger group of visually evoked startles (Preuss et al., 2006), and it might be due to either the smaller sample size or the fact that the visual evoked C-starts were tracked manually at a lower temporal resolution, relative to auditory evoked C-starts that were tracked automatically.

C-starts are not completely stereotyped, since in addition to the variation in kinematic measures they can also be followed by counterturns. This was the case with 22 of the 75 C-starts. These C-starts with counterturns were evoked by all three stimuli and looked initially similar to other C-starts but exhibited a second, slower bend, the counterturn, in the opposite direction. On average, the onset of the counterturn occurred at 34.1±1.35 ms after movement onset and it had an angular velocity of 1.3±0.12 deg. ms^{-1} with an angle of 34.5±5.29° (n=22). One notable difference between C-starts evoked by the different stimuli was that fast persistent swimming often followed startles evoked by visual looming stimuli.

Neural correlates of C-starts exhibiting counterturns

The presence of a counterturn during some C-starts raises the question of whether activity in other reticulospinal neurons precedes that counterturn. Comparison of the evoked fields in Fig. 6Ai,Bi indicates that the amplitudes of the M-spike and the initial components of the field potential associated with it varied little, with exception of the differences in the sizes of two M-spikes. However, close inspection of the later components of the recordings suggested the responses could be subdivided into two populations, one that did not exhibit significant levels of late activity and one with a marked compound response at >10 ms after the M-spike. The latter responses occurred relatively infrequently (~10% of all trials) and they could be isolated as follows: mean response and standard deviation waveforms for left- and right-directed escapes were calculated separately for each experiment (n=3). Individual responses were then compared with these averages and those that deviated appreciably from the mean ± 1 standard deviation (s.d.) for at least 5 ms were identified and the kinematics associated with the responses were analyzed. In the example of Fig. 8Ai, the evoked field potential (red) is similar to the mean potential (black, n=30 right C-starts in a single fish), and the fish executed a typical 130° C-bend but did not exhibit a counterturn, as shown in Fig. 8Aii. The example in Fig. 8Bi,ii illustrates an atypical field potential and in this case the fish performed a counterturn to the left, presumably triggered in part by the late activity in the mlf_d. Overall, analysis of the C-start escape trajectories selected on the basis of a long latency component of the corresponding field potential occurred revealed that 19/22 exhibited counterturns. The others appeared to be typical C-bends. In order to ascertain if there were other trials exhibiting counterturns that were not associated with the atypical late activity we reviewed video recordings and did not visually identify any trials with counterturns besides the 19 described above.

The above results suggest that the late responses apparent in the hindbrain evoked field potential are correlated with the occurrence of the counterturn. There were no correlations between the amplitude of the late activity and the magnitude or direction of the counterturn. However, the timing of the two responses was quite consistent. First, the latency between the onset of the largest wave in the late response (Fig. 8Bii) and that of the counterturn averaged 17.5±1.87 ms. To better quantify this relation and pool data from different fish the temporal axes of individual fish were aligned according to the onset of the initial brainstem field potential. Then 18 control responses and 18 that had counterturns were separately analyzed. To account for phase cancellation of the variable late response the root mean squared (RMS) of each field potential was calculated and averaged using a bin size of 1 ms. In trials with counterturns an additional component, as compared with the controls, was present in the interval beginning 7 ms after the onset of the field potential (Fig. 9).

The 19 C-start trials exhibiting counterturns were evoked by the full complement of stimuli used. Kinematic measurements were made for 18 of these counterturn trials. The onset of the counterturn occurred at 31.2±2.44 ms, the turn angle of the counterturn was 40±7.8°, and the maximum angular velocity of the counterturn was 1.06±0.18 deg. ms^{-1}. These values are similar to those calculated in non-implanted fish exhibiting C-starts with counterturns.

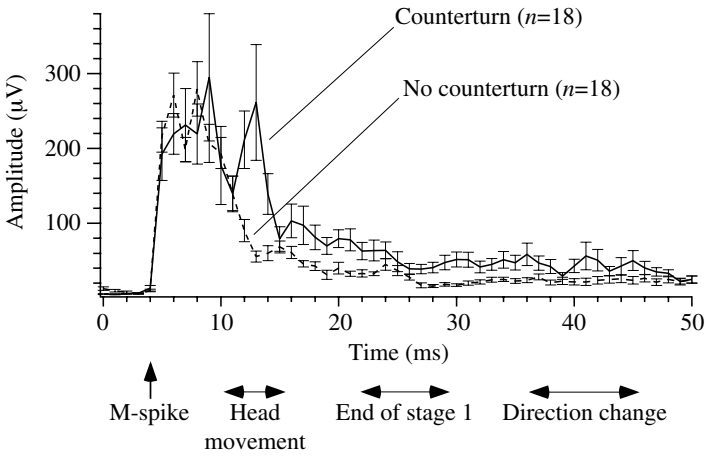

Fig. 9. Comparison of the average RMS field potentials associated with C-starts that do (solid lines) or do not (broken lines) exhibit counterturns. RMS field potentials were aligned at the onset of the individual responses. Error bars are ± 1 s.d. Horizontal arrows indicate the time sequence at which the different stages of the escape behavior take place following the onset of the M-spike (vertical arrow).

Discussion

Previous studies designed to correlate cellular activity with a defined behavior utilized chronic extracellular recordings from a single M-cell (Zottoli, 1977; Eaton et al., 1981; Canfield and Rose, 1993). Although this approach provides essential information, it was limited because correlations could be drawn only for responses in one direction and because activity of other reticulospinal neurons could not be measured. We demonstrate here that implanting a single electrode in the hindbrain allows for the discrimination of either one of the M-axons as well as detection of population activity from descending axons in the mlf_d in free-swimming goldfish. Indeed, when it was possible to distinguish right and left M-axon spikes, the direction was always predictable from the recordings. Furthermore, the longer latency activity in the mlf_d accurately predicted whether there would be a counterturn following the initial C-bend.

Discrimination of M-axon spikes

The results presented here demonstrate that the field potential preceding a C-start is long-lasting relative to the duration of a single M-spike. Nevertheless, in most experiments an initial brief component could be detected, and it could be unequivocally identified as the M-spike when the latter was recorded simultaneously with an intracellular electrode. However, in the absence of such a direct confirmation, it is difficult to be confident of M-spike identification. It remains to be seen if a different electrode design or an electrode array could improve the resolution in chronic experiments with hindbrain recordings. Regardless, it is clear that a single M-cell spike triggers C-starts for diverse stimuli, namely abrupt sound pips, ramped sound waves, and visual looming stimuli. Furthermore, in each case the hindbrain field potential that immediately follows the M-spike is generated, at least in part, by activity in a population of axons in the mlf_d and this field was stereotyped in a given fish.

It was suggested that neural activity in addition to the M-spike might correlate with C-starts having larger turn angles or angular velocities (Nissanov et al., 1990). However, the relative constancy of the hindbrain field potential, in the absence of counterturns, suggests this activity cannot be easily correlated with turn angle or angular velocity with our recordings. Nevertheless, the presence of this compound field potential, as well as the late fields that precede a counterturn, raises the question of which other neurons generate it.

Source of mlf_d activity following the M-spike

The population of neurons that direct the C-start are thought to be localized to the rhombencephalic medial reticular zone (Foreman and Eaton, 1993; O'Malley et al., 1996; Gahtan and O'Malley, 2001; Gahtan et al., 2002; Nakayama and Oda, 2004). This structure has eight segments, seven of which are clearly distinguishable (r1–r7) and an eighth consisting of a continuous column of reticulospinal neurons (Kimmel, 1982; Kimmel et al., 1982; Kimmel et al., 1985; Metcalfe et al., 1986; Lee and Eaton, 1991; Lee et al., 1993; Nakayama and Oda, 2004). Segment 4 is positioned at the level of the root of the VIIIth nerve and contains the Mauthner cells. A pair of neurons in r5 (MiD2cm) and a pair in r6 (MiD3cm) are morphologically similar to the M-cells in larval (Kimmel et al., 1982; Metcalfe et al., 1986) and adult teleost fish [zebrafish (Lee and Eaton, 1991), goldfish (Lee et al., 1993)]. The similarities include dorsal–ventral position, predominant lateral and ventral dendrites, an axon that crosses the midline and extends caudally the extent of the spinal cord (Kimmel et al., 1982; Nakayama and Oda, 2004). Consequently MiD2cm and MiD3cm are designated as M-cell homologues.

Calcium imaging studies in the larval zebrafish demonstrate that a gentle tap to the head that reliably evokes C-starts produces short-latency calcium responses in the M-cell homologues (O'Malley et al., 1996) and identified neurons in all eight hindbrain segments (Gahtan et al., 2002). It is not clear whether the tap stimulus directly excites this widespread population of neurons or if the population is activated, in part, by the M-cell or other reticulospinal neurons.

Our results are consistent with the notion that M-cell activation triggers activity in other reticulospinal neurons. That is, orthodromic activation of the M-cell by transmembrane current injection produces a field potential following the M-spike that is comparable to that produced by natural stimuli. Given the location of the recording electrode, activity in the fibers of the mlf_d are likely contributors to this triggered field potential, with a minor contribution, if any, from more distant axon tracts, such as the ventral mlf, commissural axons, axons of the lateral longitudinal fasciculus as well as interneurons and motoneurons. Furthermore, at the level of the recording site, the mlf_d contains the axons of neurons in all hindbrain segments except r1, as well as midbrain neurons of the nucleus of the mlf and local interneurons. Involvement of neurons in these brain regions would be consistent with the observations in zebrafish (O'Malley et al., 1996; Liu and Fetcho, 1999; Gahtan and O'Malley, 2001; Gahtan et al., 2002).

Based on our field recordings the duration of neural activity, *en masse*, does not exceed 8–12 ms. Furthermore, in the absence of a counterturn, there is no additional population activity. These results are consistent with the concept that the neural commands that determine the complete trajectory of a C-start are issued before the onset of forward propulsion (Eaton et al., 1988). However, counterturns that follow the initial C-bend require additional neural commands that occur later.

Counterturns or directional changes have been described previously (Foreman and Eaton, 1993) and it has been hypothesized that a population of non-Mauthner reticulospinal neurons are responsible for their initiation (Gahtan et al., 2002). Our results directly confirm that counterturns are associated with late compound field potentials in the mlf_d. As with the initial C-bend, it is not clear how angular velocity or other kinematic parameters of the counterturn are encoded.

M-cell mediation of C-starts evoked by diverse stimuli

Our data indicate that goldfish C-starts evoked by a diverse set of stimuli are, at least in their initial stages, fairly consistent with respect to measured kinematic parameters and neural

correlates. The similarities between the kinematic parameter values we have calculated and those previously published for goldfish responding to additional types of stimuli support this conclusion (Nissanov et al., 1990; Eaton and Emberley, 1991; Zottoli et al., 1999; Preuss and Faber, 2003). This finding is consistent with the notion that a single motor circuit involving the M-cell mediates all fast-starts in adult goldfish and with evidence for multimodal inputs to the M-cell (Zottoli et al., 1987; Canfield, 2003; Preuss et al., 2006; Canfield, 2006). In contrast other fish, such as the northern pike, exhibit not only C- but also S-starts, in which the fish bends in to an S-shape by contracting muscle rostrally on one side of the body and caudally on the other. The S-start is executed as both a strike and an escape and involves different neural circuits than the C-start (Hale, 2002). Differences in the escape behaviors exhibited across species may be expected, since the underlying neural circuits are thought not to be evolutionarily conserved (Hale et al., 2002). However, the possibility remains that certain as yet unknown stimuli may evoke alternative escape behaviors in goldfish that may or may not be triggered by the M-cell.

Correlating behavior with individual neurons

Bullock predicted the "*list of identifiable cells in the vertebrates will grow well beyond the Mauthner's, some Müller's, some electromotor neurons, and some spinal premotor giant cells in teleost fish*" (Bullock, 1978). Indeed he effectively anticipated the discovery of the clustering of identified neurons in the hindbrain of zebrafish and goldfish (Kimmel et al., 1982; Lee and Eaton, 1991; Lee et al., 1993). He further suggested that rather than look for unique, identifiable neurons, it might be more instructive to search for groups of neurons that are indistinguishable, for example by size and location. Perhaps such an 'equivalence size class' is represented by the axons in the mlf_d. These axons might represent functional units involved in C-starts and the contribution and timing of each might be functions of the stimulus location (Eaton and Emberly, 1991) and C-start trajectory that results, including later movements such as counterturns.

In order to test the notion that population activity recorded here might mask a more specific population code, it might be advantageous to employ electrodes, or electrode arrays, with better spatial resolution (Canfield and Mizumori, 2004). Indeed, a major advantage of this system is that a number of the reticulospinal neurons that potentially contribute to the behavior have already been identified in immobilized zebrafish (O'Malley et al., 1996; Gahtan and O'Malley, 2001; Gahtan et al., 2002) and that these neurons can be easily classified by the rhombomere in which they reside. Thus single-unit recordings from these neurons may provide clues to the specific coding strategies that determine the precise trajectory of the escape.

We thank C. Grove, T. Szabo, H. Neumeister and K. Fisher for assistance with this project and M. V. L. Bennett for providing helpful feedback on the manuscript.

References

Beall, S. P., Langley, D. J. and Edwards, D. H. (1990). Inhibition of escape tailflip in crayfish during backward walking and the defense posture. *J. Exp. Biol.* **152**, 577-582.

Bullock, T. H. (1978). Identifiable and addressed neurons in the vertebrates. In *Neurobiology of the Mauthner Cell* (ed. D. S. Faber and H. Korn), pp. 47-131. New York: Raven.

Bullock, T. H. (1990). Goals of neuroethology. *Bioscience* **40**, 244-249.

Canfield, J. G. (2003). Temporal constraints on visually directed C-start responses: behavioral and physiological correlates. *Brain Behav. Evol.* **61**, 148-158.

Canfield, J. G. (2006). Functional evidence for visuospatial coding in the Mauthner neuron. *Brain Behav. Evol.* **67**, 188-202.

Canfield, J. G. and Mizumori, S. J. (2004). Methods for chronic neural recording in the telencephalon of freely behaving fish. *J. Neurosci. Methods* **133**, 127-134.

Canfield, J. G. and Rose, G. J. (1993). Activation of Mauthner neurons during prey capture. *J. Comp. Physiol. A* **172**, 611-618.

Canfield, J. G. and Rose, G. J. (1996). Hierarchical sensory guidance of mauthner-mediated escape responses in goldfish (*Carassius auratus*) and cichlids (*Haplochromis burtoni*). *Brain Behav. Evol.* **48**, 137-156.

Deliagina, T. G., Zelenin, P. V., Fagerstedt, P., Grillner, S. and Orlovsky, G. N. (2000). Activity of reticulospinal neurons during locomotion in the freely behaving lamprey. *J. Neurophysiol.* **83**, 853-863.

Domenici, P. and Batty, R. S. (1997). Escape behavior of solitary herring (*Clupea harengus*) and comparisons with schooling individuals. *Mar. Biol.* **128**, 29-38.

Domenici, P. and Blake, R. (1997). The kinematics and performance of fish fast-start swimming. *J. Exp. Biol.* **200**, 1165-1178.

Drewes, C. D., Landa, K. B. and McFall, J. L. (1978). Giant nerve fibre activity in intact, freely moving earthworms. *J. Exp. Biol.* **72**, 217-227.

Eaton, R. C. and Emberley, D. S. (1991). How stimulus direction determines the trajectory of the Mauthner-initiated escape response in a teleost fish. *J. Exp. Biol.* **161**, 469-487.

Eaton, R. C., DiDomenico, R. and Nissanov, J. (1988). Flexible body dynamics of the goldfish C-start: implications for reticulospinal command mechanisms. *J. Neurosci.* **8**, 2758-2768.

Eaton, R. C., Lee, R. K. and Foreman, M. B. (2001). The Mauthner cell and other identified neurons of the hindbrain escape network of fish. *Prog. Neurobiol.* **63**, 467-485.

Edwards, D. H., Heitler, W. J. and Krasne, F. B. (1999). Fifty years of a command neuron: the neurobiology of escape behavior in the crayfish. *Trends Neurosci.* **22**, 153-161.

Faber, D. S. and Korn, H. (1978). Electrophysiology of the Mauthner cell: basic properties, synaptic mechanisms, and associated networks. In *Neurobiology of the Mauthner Cell* (ed. D. S. Faber and H. Korn), pp. 47-131. New York: Raven.

Foreman, M. B. and Eaton, R. C. (1993). The direction change concept for reticulospinal control of goldfish escape. *J. Neurosci.* **13**, 4101-4113.

Funch, P. G. and Faber, D. S. (1982). Action-potential propagation and orthodromic impulse initiation in Mauthner axon. *J. Neurophysiol.* **47**, 1214-1231.

Gahtan, E. and O'Malley, D. M. (2001). Rapid lesioning of large numbers of identified vertebrate neurons: applications in zebrafish. *J. Neurosci. Methods* **108**, 97-110.

Gahtan, E., Sankrithi, N., Campos, J. B. and O'Malley, D. M. (2002). Evidence for a widespread brain stem escape network in larval zebrafish. *J. Neurophysiol.* **87**, 608-614.

Hackett, J. T. and Faber, D. S. (1983). Mauthner axon networks mediating supraspinal components of the startle response in the goldfish. *Neuroscience* **8**, 317-331.

Hale, M. E. (2002). S- and C-start escape responses of the muskellunge (*Esox masquinongy*) require alternative neuromotor mechanisms. *J. Exp. Biol.* **205**, 2005-2016.

Hale, M. E., Long, J. H., Jr, McHenry, M. J. and Westneat, M. W. (2002). Evolution of behavior and neural control of the fast-start escape response. *Evolution* **56**, 993-1007.

Harper, D. G. and Blake, R. W. (1991). Prey capture and the fast start performance of Northern Pike *Esox lucius. J. Exp. Biol.* **155**, 175-192.

Kimmel, C. B. (1982). Reticulospinal and vestibulospinal neurons in the young larva of a teleost fish, *Brachydanio rerio. Prog. Brain Res.* **57**, 1-23.

Kimmel, C. B., Powell, S. L. and Kimmel, R. J. (1982). Specific reduction of development of the Mauthner neuron lateral dendrite after otic capsule ablation in *Brachydanio rerio*. *Dev. Biol.* **91**, 468-473.

Kimmel, C. B., Metcalfe, W. K. and Schabtach, E. (1985). T reticular interneurons: a class of serially repeating cells in the zebrafish hindbrain. *J. Comp. Neurol.* **233**, 365-376.

Korn, H. and Faber, D. S. (2005). The Mauthner cell half a century later: a neurobiological model for decision-making? *Neuron* **47**, 13-28.

Lee, R. K. and Eaton, R. C. (1991). Identifiable reticulospinal neurons of the adult zebrafish, *Brachydanio rerio. J. Comp. Neurol.* **304**, 34-52.

Lee, R. K., Eaton, R. C. and Zottoli, S. J. (1993). Segmental arrangement of reticulospinal neurons in the goldfish hindbrain. *J. Comp. Neurol.* **329**, 539-556.

Liu, K. S. and Fetcho, J. R. (1999). Laser ablations reveal functional relationships of segmental hindbrain neurons in zebrafish. *Neuron* **23**, 325-335.

Metcalfe, W. K., Mendelson, B. and Kimmel, C. B. (1986). Segmental homologies among reticulospinal neurons in the hindbrain of the zebrafish larva. *J. Comp. Neurol.* **251**, 147-159.

Nakayama, H. and Oda, Y. (2004). Common sensory inputs and differential excitability of segmentally homologous reticulospinal neurons in the hindbrain. *J. Neurosci.* **24**, 3199-3209.

Neumeister, H., Ripley, B., Preuss, T. and Gilly, W. F. (2000). Effects of temperature on escape jetting in the squid *Loligo opalescens*. *J. Exp. Biol.* **203**, 547-557.

Nissanov, J., Eaton, R. C. and DiDomenico, R. (1990). The motor output of the Mauthner cell, a reticulospinal command neuron. *Brain Res.* **517**, 88-98.

O'Malley, D. M., Kao, Y. H. and Fetcho, J. R. (1996). Imaging the functional organization of zebrafish hindbrain segments during escape behaviors. *Neuron* **17**, 1145-1155.

Otis, T. S. and Gilly, W. F. (1990). Jet-propelled escape in the squid *Loligo opalescens*: concerted control by giant and non-giant motor axon pathways. *Proc. Natl. Acad. Sci. USA* **87**, 2911-2915.

Preuss, T. and Faber, D. S. (2003). Central cellular mechanisms underlying temperature-dependent changes in the goldfish startle-escape behavior. *J. Neurosci.* **23**, 5617-5626.

Preuss, T. and Gilly, W. F. (2000). Role of prey-capture experience in the development of the escape response in the squid *Loligo opalescens*: a physiological correlate in an identified neuron. *J. Exp. Biol.* **203**, 559-565.

Preuss, T., Osei-Bonsu, P. E., Weiss, S. A., Wang, C. and Faber, D. S. (2006). Neural representation of object approach in a decision-making motor circuit. *J. Neurosci.* **26**, 3454-3464.

Prugh, J. I., Kimmel, C. B. and Metcalfe, W. K. (1982). Noninvasive recording of the Mauthner neurone action potential in larval zebrafish. *J. Exp. Biol.* **101**, 83-92.

Szabo, T. M., Weiss, S. A., Faber, D. S. and Preuss, T. (2006). Representation of auditory signals in the M-cell: role of electrical synapses. *J. Neurophysiol.* **95**, 2617-2629.

Wilson, D. M. (1959). Function of giant Mauthner's neurons in the lungfish. *Science* **29**, 841-842.

Wine, J. J. and Krasne, F. B. (1972). The organization of escape behavior in the crayfish. *J. Exp. Biol.* **56**, 1-18.

Zottoli, S. J. (1977). Correlation of the startle reflex and Mauthner cell auditory responses in unrestrained goldfish. *J. Exp. Biol.* **66**, 243-254.

Zottoli, S. J. and Faber, D. S. (2000). The Mauthner cell: what has it taught us? *Neuroscientist* **6**, 25-37.

Zottoli, S. J., Hordes, A. R. and Faber, D. S. (1987). Localization of optic tectal input to the ventral dendrite of the goldfish Mauthner cell. *Brain Res.* **401**, 113-121.

Zottoli, S. J., Bentley, A. P., Prendergast, B. J. and Rieff, H. I. (1995). Comparative studies on the Mauthner cell of teleost fish in relation to sensory input. *Brain Behav. Evol.* **46**, 151-164.

Zottoli, S. J., Newman, B. C., Rieff, H. I. and Winters, D. C. (1999). Decrease in occurrence of fast startle responses after selective Mauthner cell ablation in goldfish (*Carassius auratus*). *J. Comp. Physiol. A* **184**, 207-218.